# Oriented Triplet Markov Fields

Jean-Baptiste Courbot [a,b,1,*], Emmanuel Monfrini [c], Vincent Mazet [a], Christophe Collet [a]

[a] *ICube, Université de Strasbourg - CNRS, Illkirch 67412, France*
[b] *Ens de Lyon, Univ Lyon, Univ Lyon1, CNRS, CRAL UMR5574, Saint-Genis-Laval F-69230, France*
[c] *SAMOVAR, Département CITI, CNRS, Évry 91011, France*

## ABSTRACT

Hidden Markov Field modeling is widely used for image segmentation. However, it sometimes lacks power to handle complex situations, e.g. correlated noise, textures or non-stationarities. This is why Pairwise, and then Triplet Markov Fields were introduced to handle in a generic fashion more complex observations. In this paper, we tackle the problem of anisotropic image modeling by introducing an *Oriented Triplet Markov Field* model, able to explicitly deal with oriented structures. Using oriented features in the framework of Triplet Markov Field modeling, we compare the behavior of this model towards other Markovian modeling on images containing such oriented pattern. We present experiments on synthetic data for segmentation, and application to real data from remote sensing images.

© 2018 Elsevier B.V. All rights reserved.

## 1. Introduction

Markov Random Fields models have been extensively used in the literature, mainly for image segmentation, retrieving or denoising. When facing a segmentation problem, we generally search for an unobserved, *hidden* random process **X** from a noisy observation **y**. The latter is considered as a realization of a random process **Y**, whose stochastic behavior may be due to poor observation condition, missing information or imperfect imaging instrument.

This problem has traditionally been handled with Hidden Markov Fields (HMF) [1–3]. HMF modeling has been widely used for Bayesian image segmentation. This includes color [4] or multispectral [5] images, remote sensing [6], medical [7] or sonar [8] applications. Literature exhibits several extensions of HMF, including the *factorial* [9], the *double* [10], the *pairwise* [11] and *triplet* [12] Markov fields models. Many other specialized models have also been proposed, *e.g.* to handle edges [13–15], hierarchical features [8,16], multiple sensors [17] or fuzziness [18].

Pairwise Markov Fields (PMF) [11] modeling is an important improvement over HMF modeling. In PMF, the pair (**Y, X**) follows a Markov Field distribution. It is in fact a family of models offering a theoretical framework to perform Bayesian estimations. As an example, HMF are a particular case of PMF. The interest of PMF yields in the possibility to handle dependancies between the components of **X** and **Y** which are ignored in HMF. Triplet Markov Fields (TMF) modeling, introduced in the last decade [12], offer a more general framework. In TMF, a third *auxiliary* process **V** is introduced, and the triplet **T** = (**Y**, **X**, **V**) is assumed to have a Markov Field distribution. As we will see later, PMF and thus HMF are particular cases of TMF. Applications of TMF can be found for example in synthetic aperture radar image segmentation [12,19,20] and texture recognition [21].

In this paper, we investigate the joint Bayesian modeling of classes and orientations in images. Apart from edge-related Markov field models [13,14,22], few works handle images with oriented structures using Markovian modeling. We can only mention [23] in which directional fields are used to segment fingerprint images. However, considering local orientations, such as oriented textures, requires a fine modeling to provide an accurate segmentation. Besides, this would give additional information on the image features. Nevertheless, the problem is non-trivial: the literature exhibits several papers addressing it using computer vision-related methods (*e.g.* filtering [24], minimal path [25], or graph cut [26]). In the continuation of these studies, our work on a Markovian modeling aims at considering directional features in images.

This paper presents a TMF model accounting for local orientations in images. More specifically, we describe:

- the model distribution, and a method to sample it;
- a SEM-like algorithm to estimate the parameters of the triplet (**Y**, **X**, **V**) from a realization **y** of **Y** only;
- two methods to recover **X** and **V** from **Y** = **y** only;
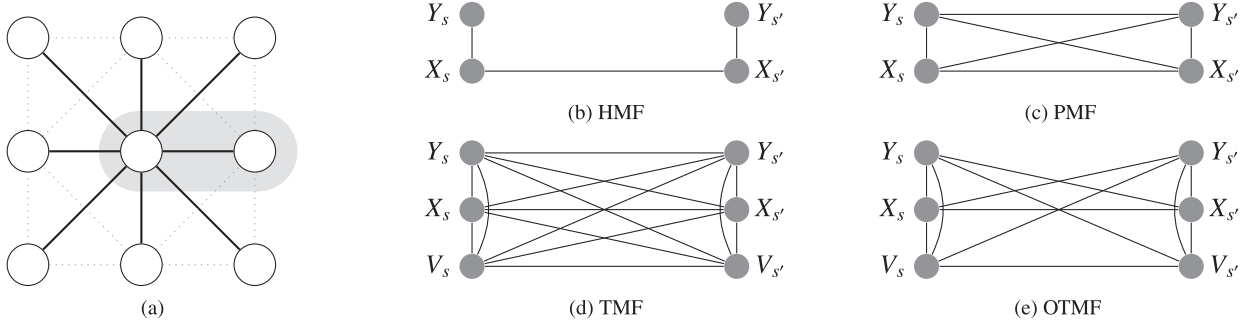- a confidence measure supplementing the segmentation ;

---

**Fig. 1.** Dependency graphs for the models mentioned in this paper. (a) Markov field relations within a local neighborhood. The plain links are related to the central site $s$, and dotted links handle other connections. (b–d) Subgraph of the links between the central site and one neighbor $s'$ (in the shaded region of (a)) within each model. Roughly speaking, eliminating a graph edge is equivalent to not account for a variable in one of the conditional distributions ruling the process (**Y, X, V**).

- experiments on synthetic images, providing quantitative segmentation results showing our TMF modeling is more robust than the classical HMF ;
- two applications on real-world images presenting directional features.

This paper extends the preliminary work published in [27] and shows results on images from real world.

It is organized as follows. We present in Section 2 the hidden, pairwise and triplet Markov Fields, as well as the Bayesian segmentation in the TMF framework. Then, we introduce a particular TMF (called OTMF for Oriented Triplet Markov Field) designed to account for local orientations in Section 3. We also describe how simulation, confidence estimation and parameter estimation are made possible. Finally, experimental results are reported in Section 4, using synthetic and real images to assess the model performances.

All along this article, a random variable (resp. vector) is noted $A$ (resp. **A**), its realization $a$ (resp. **a**), and its distribution $p(a)$ (resp. $p(\mathbf{a})$). $\mathcal{S}$ is the image lattice, containing individual pixels (or sites) $s$. The image is ruled by a neighboring system $(N_s)_{s \in \mathcal{S}}$ ; $N_s$ being the 8-neighbor set related to $s$. We also denote $\mathcal{C}$ the set of cliques of the image, a clique being either a set of mutually neighbor sites or a singleton.

## 2. From hidden to triplet Markov fields

TMF is a large family of models, containing in particular PMF and HMF as simplifications of the most general model. Indeed, concerning the modeling of the correlations between the variables of the process (**Y, X, V**), TMF allow to make fewer concessions than HMF or PMF. The probabilistic links involved in the three models are summarized in Fig. 1. The graphs illustrate the required concession to restrict the most general TMF to the most general PMF, and how PMF can be simplified to obtain HMF. They also show how TMF enrich the most popular model. In the sequel, in each site $s$ $X_s$ is discretely-valued in $\Omega_x$, and $Y_s$ takes values in $\mathbb{R}$. Then, considering an order-2 clique $c$, $\mathbf{x}_c \in \Omega_x^2$ is the set of elements from **x** in the sites covered by the clique $c \in \mathcal{C}$, and similarly for $\mathbf{y}_c \in \mathbb{R}^2$.

### 2.1. Hidden Markov fields

Let two processes be $\mathbf{X} = (X_s)_{s \in \mathcal{S}}$ and $\mathbf{Y} = (Y_s)_{s \in \mathcal{S}}$. In HMF, **X** is assumed to have a Markov field distribution [28]:

$$p(\mathbf{x}) \propto \exp \left[ -\sum_{c \in \mathcal{C}} \psi_c(\mathbf{x}_c) \right]; \tag{1}$$

where $\psi_c$ is a potential function. In the general case $\psi_c$ depends on the clique $c$ and on its shape. We consider only the shape of

$c$ and therefore have we have $\psi_c = \psi$. A common assumption in HMF is the independent noise property:

$$p(\mathbf{y}|\mathbf{x}) = \prod_{s \in \mathcal{S}} p(y_s|\mathbf{x}) \quad \text{and} \quad p(y_s|\mathbf{x}) = p(y_s|x_s) \quad \forall s \in \mathcal{S}. \tag{2}$$

The distribution of (**X, Y**) is in this case (see also Fig. 1b):

$$p(\mathbf{x}, \mathbf{y}) \propto \exp \left( -\sum_{c \in \mathcal{C}} \psi(\mathbf{x}_c) + \sum_{s \in \mathcal{S}} \ln [p(y_s|x_s)] \right). \tag{3}$$

Then, we deduce the posterior distribution $p(\mathbf{x}|\mathbf{y})$:

$$p(\mathbf{x}|\mathbf{y}) \propto \exp \left( -\sum_{c \in \mathcal{C}} \psi(\mathbf{x}_c) + \sum_{s \in \mathcal{S}} \ln [p(y_s|x_s)] \right). \tag{4}$$

The posterior $p(\mathbf{x}|\mathbf{y})$ is still a Markov distribution when **y** is fixed, enabling a Bayesian segmentation. One can thus perform the restoration of **X** from a given $\mathbf{Y} = \mathbf{y}$ using criteria such as the Maximum A Posteriori (MAP) [1] or the Marginal Posterior Mode (MPM) [3]. The model is ruled by the parameters of the prior $p(\mathbf{x})$ and the distributions $p(y_s|x_s)$. These parameters will be described later. When they are unknown, they must be estimated with dedicated methods, *e.g.* adaptations derived from Expectation-Maximization (EM) [29,30], Stochastic EM (SEM) [31] or Iterative Conditional Estimation (ICE) [32] algorithms.

When considering the image segmentation, HMF are considered robust to numerous situations [1–4,6–8]. The modeling is challenged by images presenting textures, fuzziness or, more generally, when the noise is correlated. This is likely because the HMF assumptions (2) are too strong to handle complex noise. Works of [18], among others, show that classical HMF can be extended on a case-by-case basis.

### 2.2. Pairwise Markov fields

In PMF, the model of $p(\mathbf{y}|\mathbf{x})$ is enriched. Indeed, assuming that (**X, Y**) is a PMF means that $\mathbf{Z} = (\mathbf{X}, \mathbf{Y})$ has a Markov Field distribution (see Fig. 1c):

$$p(\mathbf{z}) \stackrel{\Delta}{=} p(\mathbf{x}, \mathbf{y}) \propto \exp \left[ -\sum_{c \in \mathcal{C}} \Psi(\mathbf{z}_c) \right]; \tag{5}$$

where $\mathbf{z}_c = (\mathbf{x}_c, \mathbf{y}_c) \in (\Omega_x \times \mathbb{R})^2$. Let us remark that the HMF distribution (3) is a particular case of the PMF distribution (5). Besides, the posterior $p(\mathbf{x}|\mathbf{y})$ is still a Markov Field [11], enabling a general formulation for the MAP [1] and MPM [3] estimators. When the parameters are unknown, they must be estimated using methods generalizing the HMF version of EM, SEM or ICE for example.

## 2.3. Triplet Markov fields

The particularity of TMF resides in the introduction of a third auxiliary process $\mathbf{V} = (V_s)_{s \in \mathcal{S}}$ supplementing $\mathbf{X}$ and $\mathbf{Y}$, where $V_s$ is discretely-valued in $\Omega_v$.

In TMF, $\mathbf{T} = (\mathbf{Y}, \mathbf{X}, \mathbf{V})$ is a Markov field (see Fig. 1d):

$$p(\mathbf{t}) \triangleq p(\mathbf{y}, \mathbf{x}, \mathbf{v}) \propto \exp\left[ -\sum_{c \in \mathcal{C}} \phi(\mathbf{y}_c, \mathbf{x}_c, \mathbf{v}_c) \right]; \qquad (6)$$

where $\mathbf{v}_c \in \Omega_v^2$. This generalizes PMF since the distribution (5) is a particular case of (6). Furthermore, the pair $(\mathbf{X}, \mathbf{Y})$ is no longer assumed to be a PMF.

In TMF, the $\mathbf{V}$ process may have several interpretations, which have to be thoroughly specified in the model formulation. For instance, it has been used in the literature to model textures [12,21], but could also be used to describe latent phenomena with no direct interpretation in the observed images.

Besides, the posterior $p(\mathbf{x}, \mathbf{v}|\mathbf{y})$ is a Markov distribution:

$$p(\mathbf{x}, \mathbf{v}|\mathbf{y}) \propto \exp\left[ -\sum_{c \in \mathcal{C}} \phi(\mathbf{y}_c, \mathbf{x}_c, \mathbf{v}_c) \right]. \qquad (7)$$

This enables the Bayesian segmentation of images [1,3]. Let us describe more specifically the MAP criterion [1]:

$$(\hat{\mathbf{x}}, \hat{\mathbf{v}})^{MAP} = \underset{(\boldsymbol{\omega}, \boldsymbol{v}) \in (\Omega_x \times \Omega_v)^{|\mathcal{S}|}}{\arg\max} \; p(\mathbf{X} = \boldsymbol{\omega}, \mathbf{V} = \boldsymbol{v}|\mathbf{Y} = \mathbf{y}). \qquad (8)$$

On the other hand, the MPM criterion [3] yields:

$$\forall s \in \mathcal{S}, (\hat{x}_s, \hat{v}_s)^{MPM} = \underset{(\omega, v) \in \Omega_x \times \Omega_v}{\arg\max} \; p(X_s = \omega, V_s = v|\mathbf{Y} = \mathbf{y}). \qquad (9)$$

The exact distributions $p(\mathbf{x}, \mathbf{v}|\mathbf{y})$ and $p(x_s, v_s|\mathbf{y})$ are known only up to a constant. Realizations can however be simulated, using Gibbs [1,33] or Metropolis–Hastings [33,34] algorithms. The MAP segmentation can be approximated by the iterative conditional modes [2] algorithm, and the MPM segmentation can be computed using an adaptation of Marroquin's algorithm [3].

Parameter estimation is not trivial in HMF-based models, and is harder in TMF-based models. Indeed, let us recall that we seek at inferring the distribution of $(\mathbf{Y}, \mathbf{X}, \mathbf{V})$ from the single $\mathbf{Y} = \mathbf{y}$ ; and that the triplet distribution is only known up to a constant. Methods based on the stochastic gradient [35] or Gibbsian EM [36] propose solutions to estimate parameters. For robustness reasons [37,38], we choose to use in this paper a method derived from the stochastic variant of EM called SEM, which is described later in the OTMF framework.

## 3. Oriented triplet Markov fields

This section introduces a particular TMF designed to model images presenting directional features. The probabilistic links involved in this model are reported in Fig. 1e.

### 3.1. Model

Let $\mathbf{T} = (\mathbf{Y}, \mathbf{X}, \mathbf{V})$ be a stationary TMF (6), where $\mathbf{V}$ models the privileged orientations in $\mathbf{X}$. Since $\mathbf{T}$ has a Markov distribution, it is described in each site $s$ by $p(t_s|\mathbf{t}_{N_s})$. We assume that $\mathbf{T}_s$ and $\mathbf{Y}_{N_s}$ are independent given $(\mathbf{X}_{N_s}, \mathbf{V}_{N_s})$. Hence:

$$\begin{aligned} p(\mathbf{t}_s|\mathbf{t}_{N_s}) &= p(\mathbf{t}_s|\mathbf{x}_{N_s}, \mathbf{v}_{N_s}) \\ &= p(y_s|\mathbf{x}_{N_s}, \mathbf{v}_{N_s}, x_s, v_s) \\ &\quad \times p(x_s|\mathbf{x}_{N_s}, \mathbf{v}_{N_s}, v_s) p(v_s|\mathbf{x}_{N_s}, \mathbf{v}_{N_s}). \end{aligned} \qquad (10)$$

$V_s$ and $\mathbf{X}_{N_s}$ are independent given $\mathbf{V}_{N_s}$. The third term of (10) becomes:

$$p(v_s|\mathbf{x}_{N_s}, \mathbf{v}_{N_s}) = p(v_s|\mathbf{v}_{N_s}). \qquad (11)$$
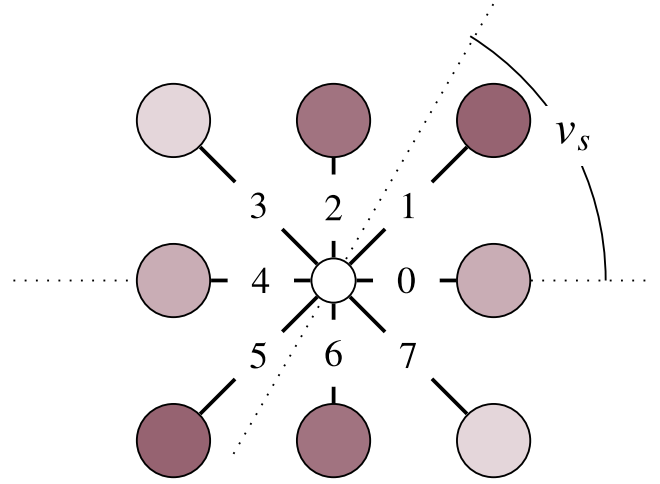


**Fig. 2.** Neighbor indexing and local orientation measurement within a local neighborhood. Site darkness is proportional to the output of the orientation function $\varphi^k$ with $k \in N_s$ from (15) with respect to $v_s = \pi/3$.

$X_s$ and $\mathbf{V}_{N_s}$ are independent given $(\mathbf{X}_{N_s}, V_s)$. The second term of (10) becomes:

$$p(x_s|\mathbf{x}_{N_s}, \mathbf{v}_{N_s}, v_s) = p(x_s|\mathbf{x}_{N_s}, v_s). \qquad (12)$$

These assumptions are illustrated in Fig. 1e.

We now specify the distributions (11), (12), and the first term of (10):

- $\mathbf{V}$ having a Markov Field distribution, (11) relies on the following Potts potentials:

$$p(v_s|\mathbf{v}_{N_s}) \propto \exp\left( -\alpha \sum_{s' \in N_s} [1 - 2\delta_{v_s}(v_{s'})] \right); \qquad (13)$$

where $\delta_{v_s}$ is the Dirac measure for $v_s$.

- $p(\mathbf{x}|\mathbf{v})$ is a Markov Field distribution, so (12) relies on:

$$p(x_s|\mathbf{x}_{N_s}, v_s) \propto \exp\left( -\beta \sum_{s' \in N_s} \varphi^{s'}(v_s)[1 - 2\delta_{x_s}(x_{s'})] \right). \qquad (14)$$

where the *orientation function* $\varphi^k$ is introduced to handle the orientations within local neighborhood. In the case of a 8-neighborhood, $N_s = \{0, \dots, 7\}$ as in Fig. 2. When considering only slope and order-2 cliques, the contribution of the orientations can be considered with:

$$\varphi^k(v) = \left| \cos\left( v - \frac{k\pi}{4} \right) \right| \qquad (15)$$

Note that we could use $\varphi^k(v) = 1 + \cos\left( v - \frac{k\pi}{4} \right)$ to consider both slope and directions.

- To provide a more intuitive formulation of $p(y_s|\mathbf{x}_{N_s}, \mathbf{v}_{N_s}, x_s, v_s)$, we assume that the first term of (10) can be split into:

$$p(y_s|\mathbf{x}_{N_s}, \mathbf{v}_{N_s}, x_s, v_s) \propto f(x_s, y_s) g(x_s, v_s, \mathbf{x}_{N_s}, \mathbf{v}_{N_s}). \qquad (16)$$

A particular care is required to define $f$ regarding the considered application: it has to be determined according to the chosen noise model. In the sequel, $f$ is assumed to be a Gaussian with mean $\mu_{x_s}$ and variance $\sigma_{x_s}^2$, which is known to be suitable for many natural image segmentation cases [1–3].

Besides, $g(x_s, v_s, \mathbf{x}_{N_s}, \mathbf{v}_{N_s})$ is a distribution related to neighborhood configurations within $\mathbf{X}$ and $\mathbf{V}$ (number of neighbors identical to the central site value). We assume it is written as:

$$g(x_s, v_s, \mathbf{x}_{N_s}, \mathbf{v}_{N_s}) \propto \sum_{(s', r') \in N_s^2} \delta_{x_s, v_s}(x_{s'}, v_{r'}). \qquad (17)$$

Hence, $g$ allows to weight the contributions of $f(x_s, y_s)$ with respect to neighbor configurations, without dramatically raising the complexity of $p(y_s|\mathbf{x}_{N_s}, \mathbf{v}_{N_s}, x_s, v_s)$.

**Remark 1.** The orientation function $\varphi$ (15) can be generalized to 3D modeling and a 26-neighborhood for example or extended to higher-order cliques.

To sum up, the distribution $p(\mathbf{t}_s|\mathbf{t}_{N_s})$ ruling **T** is now written:

$$p(\mathbf{t}_s|\mathbf{t}_{N_s}) \propto \exp\left(-\frac{(y_s - \mu_{x_s})^2}{2\sigma_{x_s}^2}\right) \sum_{(s',r') \in N_s^2} \delta_{x_s, v_s}(x_{s'}, v_{r'})$$

$$\times \exp\left(-\alpha \sum_{s' \in N_s}[1 - 2\delta_{v_s}(v_{s'})] - \beta \sum_{s' \in N_s} \varphi^{s'}(v_s)[1 - 2\delta_{x_s}(x_{s'})]\right). \quad (18)$$

Realizations of **T** can be performed through Gibbs sampling [1,33]. In practice, we use the *chromatic* Gibbs sampler [39], allowing to perform simultaneous sampling on grids ("colors") of mutually non-neighbor elements, while preserving the Gibbs sampler ergodicity.

One can also sample marginals of the triplet distribution. This is of interest in two cases, among others:

1. sampling the posterior distribution $p(\mathbf{x}, \mathbf{v}|\mathbf{y})$ from (7) for segmentation purpose (see Section 2.3);
2. sampling $p(\mathbf{x}, \mathbf{y}|\mathbf{v})$ to simulate a synthetic image (as in Section 4.1).

**Remark 2.** In the most general case, the triplet distribution can be written $p(\mathbf{t}) = p(\mathbf{y}, \mathbf{x}, \mathbf{v}) = p(\mathbf{y}|\mathbf{x}, \mathbf{v})p(\mathbf{x}|\mathbf{v})p(\mathbf{v})$. In the proposed model, $p(\mathbf{y}|\mathbf{x}, \mathbf{v})$, $p(\mathbf{x}|\mathbf{v})$, and $p(\mathbf{v})$ are Markov field distributions.

### 3.2. Segmentation and confidence

We investigate in this section the use of a point-wise confidence measure. Such a measure can easily be computed thanks to the MPM framework. By construction, the MPM estimators of $X_s$, $V_s$ are the most likely classes with respect to the posterior distribution $p(x_s, v_s|\mathbf{y})$. This choice is a hard decision, and therefore does not reflect the confidence of the segmentation. Indeed, several situations can be encountered, among which:

- the most favorable case: the chosen class is largely more likely than the other classes,
- harder cases, in which the gap between probabilities is small.

Hence, we supplement the segmentation by introducing a confidence measure $\mathbf{u} = (\mathbf{u}^x, \mathbf{u}^v)$ based on the difference between the MPM output and the others, rejected outputs. $\forall s \in \mathcal{S}$:

$$\begin{cases} u_s^x = \min_{\omega \neq \hat{x}_s^{\mathrm{MPM}}}\left[p(X_s = \hat{x}_s^{\mathrm{MPM}}|\mathbf{y}) - p(X_s = \omega|\mathbf{y})\right]; \\ u_s^v = \min_{\nu \neq \hat{v}_s^{\mathrm{MPM}}}\left[p(V_s = \hat{v}_s^{\mathrm{MPM}}|\mathbf{y}) - p(V_s = \nu|\mathbf{y})\right]. \end{cases} \quad (19)$$

This yields two *confidence maps* $\mathbf{u}^x = (u_s^x)_{s \in \mathcal{S}}$ and $\mathbf{u}^v = (\mathbf{u}_s^v)_{s \in \mathcal{S}}$. They take values in [0, 1], 0 and 1 corresponding respectively to the most weakly and strongly confident cases.

Finally, let us remark that the introduced confidence measure is of particular interest when segmenting orientations from an image without directional features, hence yielding high uncertainties.

### 3.3. Parameter estimation

From (18), the model is ruled by $\alpha$, $\beta$, $g$ and the $K = |\Omega_x|$ means $\mu_{x_s}$ and $K$ variances $\sigma_{x_s}^2$ which parametrize $f$. We note $\Theta$ the complete parameter set. Let us notice that the parameters do not depend on the site $s$ since **T** is stationary.

#### 3.3.1. Supervised estimation

In this paragraph, the complete $(\mathbf{y}, \mathbf{x}, \mathbf{v})$ is assumed available. The $K$ means $\mu_{x_s}$ and variances $\sigma_{x_s}^2$ are estimated with standard Maximum Likelihood Estimators (MLE) [40]. Besides, the parameter $\alpha$ and $\beta$ are estimated thanks to **v** and **x** respectively, with the least-square estimator of [41]. Lastly, $g(x_s, v_s, \mathbf{x}_{N_s}, \mathbf{v}_{N_s})$ is estimated by the normalized histogram:

$$\hat{g}(x_s, v_s, \mathbf{x}_{N_s}, \mathbf{v}_{N_s}) = \frac{1}{|\mathcal{S}'|} \sum_{r \in \mathcal{S}'} \mathbb{I}_{h_{r,N_r} = h_{s,N_s}}; \quad (20)$$

where

$$h_{s,N_s} = \sum_{(s',r') \in N_s^2} \delta_{x_s, v_s}(x_{s'}, v_{r'}) \quad (21)$$

and $\mathcal{S}'$ is the lattice $\mathcal{S}$ without the edge, since the sites on the edge do not have 8 neighbors.

**Remark 3.** In practice, the indicator functions sum may be zero-valued in estimators (20). This can impede simulations by forbidding rare configurations to occur. Instead, the estimation is set to a small value.

#### 3.3.2. Unsupervised estimation

In image segmentation, complete data are seldom available. Since only $\mathbf{Y} = \mathbf{y}$ is available, we use an adaptation of the SEM algorithm [31] which allows, at each iteration, a parameter re-estimation directly from complete data thanks to realization of the missing data, simulated using parameters estimated at the previous step. At each iteration $k$, let $\hat{\Theta}^k$ be the parameter set to be estimated at this iteration, we have to:

1. compute $p_{\hat{\Theta}^{k-1}}(\mathbf{x}, \mathbf{v}|\mathbf{y})$ (Expectation step). This distribution is sampled with the help of several independent Gibbs sampling ;
2. simulate $(\mathbf{x}^k, \mathbf{v}^k)$ along $p_{\hat{\Theta}^{k-1}}(\mathbf{x}, \mathbf{v}|\mathbf{y})$ (Stochastic step);
3. estimate $\hat{\Theta}^k$ using the estimators described in Section 3.3.1.

**Remark 4.** Strictly speaking, this algorithm only approximates the SEM algorithm, in which only MLE are used at step 3. Since MLE are not available for $\alpha$, $\beta$ and $g(x_s, v_s, \mathbf{x}_{N_s}, \mathbf{v}_{N_s})$ we used the estimators described in Section 3.3.1.

To sum up, one can estimate parameters in the OTMF framework in an unsupervised fashion. Hence, OTMF enables the joint unsupervised segmentation of orientations and classes in images.

## 4. Experiments

This section reports experiments concerning segmentation of synthetic and real images using the proposed OTMF model. Considering that removing the auxiliary process **V** from the proposed model reduces it to a classical HMF model, we use the latter as a baseline for comparison.

### 4.1. Synthetic images segmentation

First, we evaluate the model performance by segmenting synthetic images with known ground truths. In this section, we set $\Omega_x = \{\omega_0, \omega_1\}$, $\Omega_v = \{v_0, v_1\} = \{\pi/4, 3\pi/4\}$. Two experiments are set, increasing the difficulty with respect to the model hypothesis:

A. **v** has four defined quadrants and **x, y** are sampled conditionally to **v** (see Fig. 3a–c);
B. **v** is unknown, **x** is set to present directional features (see Fig. 4a, b).

The noise distribution is a Gaussian mixture with means $\mu_0 = 0$, $\mu_1 = 1$, and standard deviations $\sigma_0 = \sigma_1 = \sigma$. Several settings are investigated:
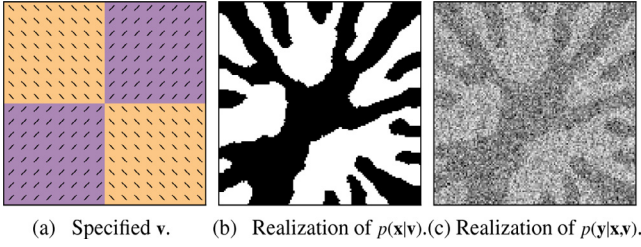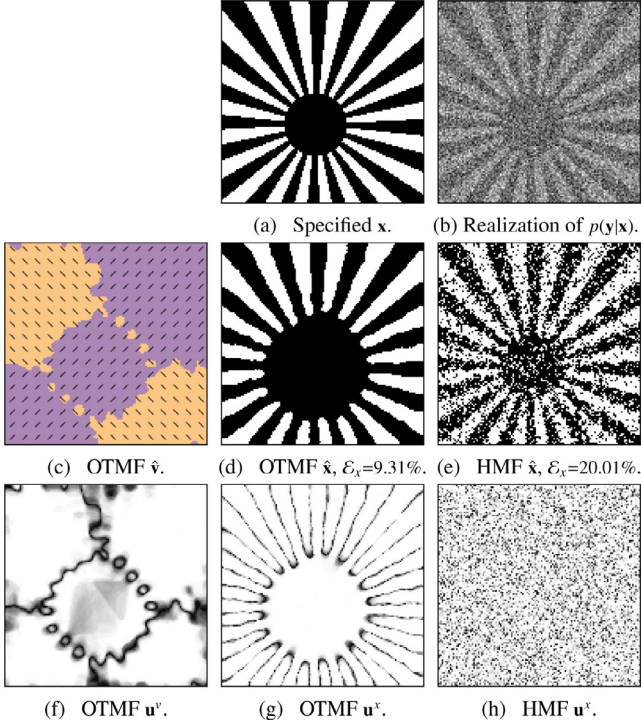
(a) Specified **v**.  (b) Realization of $p(\mathbf{x}|\mathbf{v})$.(c) Realization of $p(\mathbf{y}|\mathbf{x},\mathbf{v})$.

**Fig. 3.** Experiment A with $\sigma = 1.0$.



(a) Specified **x**.  (b) Realization of $p(\mathbf{y}|\mathbf{x})$.

(c) OTMF **v̂**.  (d) OTMF **x̂**, $\mathcal{E}_x$=9.31%. (e) HMF **x̂**, $\mathcal{E}_x$=20.01%.

(f) OTMF **u**$^v$.  (g) OTMF **u**$^x$.  (h) HMF **u**$^x$.

**Fig. 4.** Experiment B with $\sigma = 1.0$, and the corresponding unsupervised results using the MPM criterion. In the confidence maps, black pixels are zero-valued and white pixels are valued to one. In this case, the OTMF confidence maps **u**$^v$ and **u**$^x$ clearly depict class contour, related to stationarity changes in the underlying process.

- Supervised *vs.* unsupervised segmentation ;
- Low ($\sigma = 0.5$) and high ($\sigma = 1.0$) noise levels (yielding respectively signal-to-noise ratios of 0.0 dB and −6.0 dB);
- MAP (8) and MPM (9) segmentation criteria.

Segmentations with HMF are also performed in the same conditions. Averaging over 100 noise realizations, the performance evaluation is based on the error rates, noted $\mathcal{E}_x$ and $\mathcal{E}_v$. Fig. 4e–f exemplify the MPM segmentation results, and the complete measures are reported in Table 1.

**OTMF *vs*. HMF.** In all considered cases, the OTMF-based segmentation yields equally or significantly better results than the HMF-based method.

Indeed, in the easier case (Exp. A and $\sigma = 0.5$) weak noise enhances the segmentation for HMF, yielding quite as good results as OTMF. In the other cases, the improvement gap ranges from 1.90% to 24.23%.

**MAP *vs*. MPM.** Within OTMF, the results suggest that the MAP segmentation of **x** outperforms its MPM counterpart in most cases. Let us remark that this is not true within the HMF framework; the best HMF results being provided by MPM segmentation. Besides, we also notice that in TMF the best segmentations of **v** are pro-
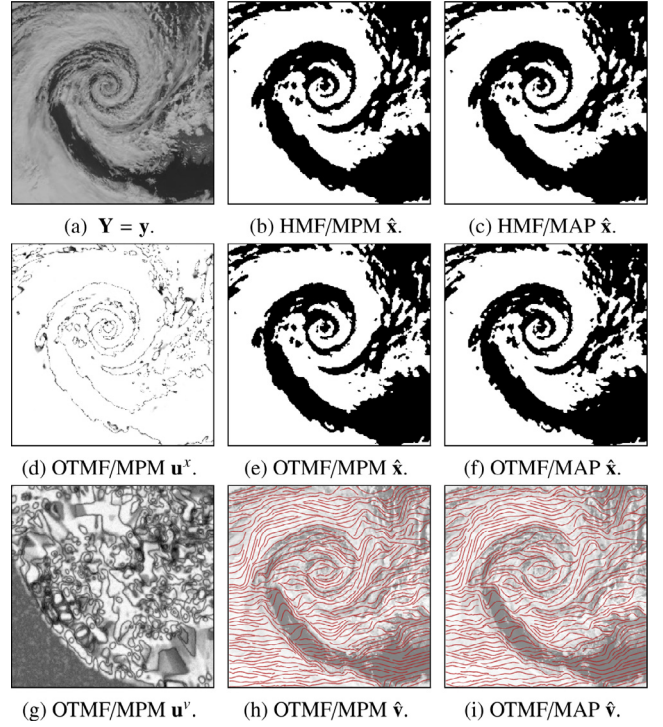


(a) **Y = y**.  (b) HMF/MPM **x̂**.  (c) HMF/MAP **x̂**.

(d) OTMF/MPM **u**$^x$.  (e) OTMF/MPM **x̂**.  (f) OTMF/MAP **x̂**.

(g) OTMF/MPM **u**$^v$.  (h) OTMF/MPM **v̂**.  (i) OTMF/MAP **v̂**.

**Fig. 5.** Low pressure system remote sensing image, covering clouds of varying direction. In the confidence maps **u**$^x$ and **u**$^v$, low (resp. high) values are depicted in black (resp white). The orientations are depicted by the red curves superimposed on **Y = y**, so that the orientations are tangent to each curve. (For interpretation of the references to colour in this figure legend, the reader is referred to the web version of this article.)

vided by the MPM, with significant gains ranging from 1.73% to 5.09%.

**Retrieving orientations.** Errors on the OTMF-based segmentation of **v** are non-negligible. However, a precise estimation of the directions seems out of reach: indeed, the baseline in the easier case (supervised Exp. A, with $\sigma = 0.5$) is an average 24.00% error rate. This may be induced by wide, homogeneous regions presenting low segmentation confidence, meaning that the choice was harder to perform (see next section). This also mean that the method is very robust to variations of **v**, since the error rates on **x** are still satisfying.

### 4.2. Real images segmentation

The problem of jointly segmenting **x** and **v** can arise in a remote sensing framework, in which artificial or natural structures strongly influence the image composition. We present in this section two segmentation examples using real images, within the HMF and OTMF framework, and with both MPM and MAP segmentation criterion. These examples are complimentary, and show the possible gain over HMF in terms of orientation retrieval and in terms of segmentation quality. We set $|\Omega_v| = 6$ with $\Omega_v = \{\pi/12, 3\pi/12, \ldots, 11\pi/12\}$.

#### 4.2.1. Low-pressure system

Fig. 5a depicts a remote sensing image of a meteorological phenomenon called *low-pressure system* acquired over Iceland by NASA's Aqua/MODIS satellite (public domain). Two main classes are visible: the clouds and the remaining of the image, so we set $|\Omega_x| = 2$. The former is noised by intensity variations, and the latter by small clouds and Iceland in the bottom right of the image.

Fig. 5g–i present the segmentation results with the OTMF model, and the related confidence maps associated to the MPM

**Table 1**
Experimental segmentation results, averaging over 100 different noise realizations. We compare four values of the error rate $\mathcal{E}_x$ and two values of $\mathcal{E}_v$, which are all in percent. Measures with a significant improvement (above 1%) above the other results are reported in bold.

| | | | HMF | | OTMF | | | |
| | | | MPM | MAP | MPM | | MAP | |
| | Exp. | $\sigma$ | $\mathcal{E}_x$ | $\mathcal{E}_x$ | $\mathcal{E}_x$ | $\mathcal{E}_v$ | $\mathcal{E}_x$ | $\mathcal{E}_v$ |
|---|---|---|---|---|---|---|---|---|
| Supervized | A | 0.5 | 1.24 | 2.73 | 1.25 | **24.00** | 0.89 | 28.10 |
| | | 1.0 | 5.07 | 4.99 | 4.62 | **26.41** | **1.55** | 28.14 |
| | B | 0.5 | 3.21 | 2.33 | 3.11 | – | 1.54 | – |
| | | 1.0 | 14.46 | 12.91 | 10.29 | – | **3.57** | – |
| Unsuperv. | A | 0.5 | 1.21 | 2.40 | 1.27 | **24.12** | 1.30 | 29.21 |
| | | 1.0 | 21.96 | 21.72 | 17.92 | 34.33 | **15.39** | 34.69 |
| | B | 0.5 | 8.24 | 15.16 | **3.04** | – | 7.91 | – |
| | | 1.0 | 23.93 | 23.57 | 22.03 | – | **20.23** | – |

segmentations. The HMF segmentations with the same settings are also reported in Fig. 5b and c for comparison. Several comments can be made :

- both OTMF and HMF segmentations of **x** seem to detect the main features of the image. The differences consist mainly in several small features appearing in the OTMF segmentation and not in its HMF counterpart;
- the confidence map $\mathbf{u}^x$ related to the MPM segmentation of **x** well describes the difficulties encountered in the Markovian modeling to handle changes in stationarity (*e.g.*, borders). They also indicate that the regions within these border should be correctly segmented;
- results concerning the orientations retrieval in the OTMF-based segmentations of **v** seem particularly striking. Indeed, most of the segmented orientations seem to capture features from the original image;
- the confidence map $\mathbf{u}^v$ (associated to the MPM estimate $\hat{\mathbf{v}}$) shows the stationarity changes for **v**. Ambiguous regions (*e.g.* bottom left corner) are well captured and may be used to identify which regions are less relevant to the search for orientation.

### 4.2.2. Vine remote sensing images

Fig. 6a depicts a panchromatic image of a vineyard from the Pléiades system [42] acquired over Alsace, France in 2012. It presents several directional features which seems homogeneous within wide image regions, while abruptly varying between these regions. To account for the various intensities, we set $|\Omega_x| = 3$ classes.

Fig. 6b–i depict the HMF-based segmentation, OTMF-based segmentations and related confidence maps (when relevant). The following comments can be made:

- the OTMF-based segmentations of **x** seem to correctly capture the visible features in the image. The differences with the HMF segmentation are particularly striking: the latter seemingly fails to handle a large number of small features, both with MPM and MAP criterion;
- the OTMF-based segmentations of **v** present several coherent regions, which seems relevant to both the corresponding stationarities of $\hat{\mathbf{x}}$ and the apparent directional features of **y**;
- the confidence map $\mathbf{u}^v$ provides here also additional information: it bolsters the hypothesis of privileged direction in some regions (the vine crops) in contrast to others (*e.g*, the track).

## 5. Conclusion

In this paper, we presented a TMF model considering jointly, in a new way, signal classes and orientations within an image.



(a) $\mathbf{Y} = \mathbf{y}$.    (b) HMF/MPM $\hat{\mathbf{x}}$.    (c) HMF/MAP $\hat{\mathbf{x}}$.

(d) OTMF/MPM $\mathbf{u}^x$.    (e) OTMF/MPM $\hat{\mathbf{x}}$.    (f) OTMF/MAP $\hat{\mathbf{x}}$.

(g) OTMF/MPM $\mathbf{u}^v$.    (h) OTMF/MPM $\hat{\mathbf{v}}$.    (i) OTMF/MAP $\hat{\mathbf{v}}$.
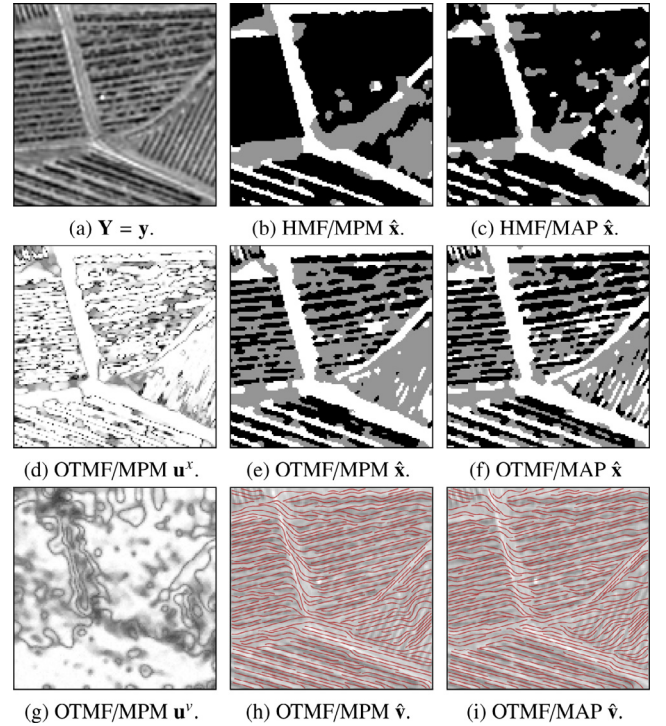
**Fig. 6.** Pléiades panchromatic image (0.5 m) [42], covering vine crops of different orientation, due to terrain. ©CNES 2012, distribution Astrium Services, France, all rights reserved. The legend is the same as in Fig. 5.

We detailed how simulation, parameter estimation and joint signal/orientation segmentation are made possible within the model we proposed. Additional estimations concerning the segmentation quality were also introduced and experiments show the model to be relevant to the considered problem, and more efficient than its HMF counterpart. The algorithm behavior yields satisfactory results.

Future works on this topic could consider the use of an additional "magnitude" component (see *e.g.* [43]), yielding bivariate values for **V**. If this component is discretely-valued and bounded, the segmentation and estimation techniques are identical to those presented in this paper. An other point of interest is the use of continuous values for **V**, which would require other techniques for segmentation. In the spirit of research reproducibility, the source code of our experiments will be made available online.

## Acknowledgments

## References

[1] S. Geman, D. Geman, Stochastic relaxation, Gibbs distributions, and the Bayesian restoration of images, IEEE Trans. Pattern Anal. Mach. Intell. 6 (1984) 721–741.
[2] J. Besag, On the statistical analysis of dirty pictures, J. Roy. Stat. Soc. B. Met. (1986) 259–302.
[3] J. Marroquin, et al., Probabilistic solution of ill-posed problems in computational vision, J. Am. Stat. Assoc. 82 (397) (1987) 76–89.
[4] Z. Kato, T.-C. Pong, A Markov random field image segmentation model for color textured images, Image Vis. Comp. 24 (10) (2006) 1103–1114.
[5] F. Salzenstein, C. Collet, Fuzzy Markov random fields versus chains for multispectral image segmentation, IEEE Trans. Pattern Anal. Mach. Intell. 28 (11) (2006) 1753–1767.
[6] R. Fjortoft, et al., Unsupervised classification of radar images using hidden Markov chains and hidden Markov random fields, IEEE IEEE Trans. Geosci. Remote Sens. 41 (3) (2003) 675–686.
[7] Y. Zhang, et al., Segmentation of brain MR images through a hidden Markov random field model and the expectation-maximization algorithm, IEEE Trans. Med. Imag 20 (1) (2001) 45–57.
[8] M. Mignotte, et al., Sonar image segmentation using an unsupervised hierarchical MRF model, IEEE Trans. Image Process. 9 (7) (2000) 1216–1231.
[9] J. Kim, R. Zabih, Factorial Markov random fields, in: ECCV, Springer, 2002, pp. 321–334.
[10] D.E. Melas, S.P. Wilson, Double Markov random fields and Bayesian image segmentation, IEEE Trans. Signal Process. 50 (2) (2002) 357–365.
[11] W. Pieczynski, A.-N. Tebbache, Pairwise Markov random fields and segmentation of textured images, Machine Graph. Vis. 9 (3) (2000) 705–718.
[12] D. Benboudjema, W. Pieczynski, Unsupervised statistical segmentation of nonstationary images using triplet Markov fields, IEEE Trans. Pattern Anal. Mach. Intell. 29 (8) (2007) 1367–1378.
[13] X. Descombes, et al., Fine structures preserving Markov model for image processing, SCIA, 1995.
[14] P.C. Smits, S.G. Dellepiane, Synthetic aperture radar image segmentation by a detail preserving Markov random field approach, IEEE Trans. Geosci. Remote Sens. 35 (4) (1997) 844–857.
[15] J. August, S.W. Zucker, Sketches with curvature: the curve indicator random field and Markov processes, IEEE Trans. Pattern Anal. Mach. Intell. 25 (4) (2003) 387–400.
[16] M.S. Crouse, et al., Wavelet-based statistical signal processing using hidden Markov models, IEEE Trans. Signal Process. 46 (4) (1998) 886–902.
[17] A. Bendjebbour, et al., Multisensor image segmentation using Dempster-Shafer fusion in Markov fields context, IEEE Trans. Geosci. Remote Sens. 39 (8) (2001) 1789–1798.
[18] F. Salzenstein, W. Pieczynski, Parameter estimation in hidden fuzzy Markov random fields and image segmentation, Graph. Models Image Process. 59 (4) (1997) 205–220.
[19] P. Zhang, et al., Unsupervised multi-class segmentation of SAR images using fuzzy triplet markov fields model, Pattern Recog. 45 (11) (2012) 4018–4033.
[20] Y. Wu, et al., Unsupervised multi-class segmentation of SAR images using triplet Markov fields models based on edge penalty, Pattern Recog. Lett. 32 (11) (2011) 1532–1540.
[21] J. Blanchet, F. Forbes, Triplet Markov fields for the classification of complex structure data, IEEE Trans. Pattern Anal. Mach. Intell. 30 (6) (2008) 1055–1067.
[22] X. Yang, J. Liu, Unsupervised texture segmentation with one-step mean shift and boundary Markov random fields, Pattern Recog. Lett. 22 (10) (2001) 1073–1081.
[23] S.C. Dass, Markov random field models for directional field and singularity extraction in fingerprint images, IEEE Trans. Image Process. 13 (10) (2004) 1358–1367.
[24] R. Rigamonti, V. Lepetit, Accurate and efficient linear structure segmentation by leveraging ad hoc features with learned filters, in: MICCAI, Springer, 2012, pp. 189–197.
[25] F. Benmansour, L.D. Cohen, Tubular structure segmentation based on minimal path method and anisotropic enhancement, Int. J. Comput. Vis. 92 (2) (2011) 192–210.
[26] C. Bauer, et al., Segmentation of interwoven 3D tubular tree structures utilizing shape priors and graph cuts, Med. Image Anal. 14 (2) (2010) 172–184.
[27] J.-B. Courbot, et al., Oriented Triplet Markov fields for hyperspectral image segmentation, WHISPERS, IEEE, 2016.
[28] P. Fieguth, Statistical Image Processing and Multidimensional Modeling, Springer Science & Business Media, 2010.
[29] A.P. Dempster, et al., Maximum likelihood from incomplete data via the EM algorithm, J. Roy. Stat. Soc. B. Met. (1977) 1–38.
[30] G. McLachlan, T. Krishnan, The EM Algorithm and Extensions, 382, John Wiley & Sons, 2007.
[31] G. Celeux, J. Diebolt, A stochastic approximation type EM algorithm for the mixture problem, Stochastics 41 (1–2) (1992) 119–134.
[32] Y. Delignon, et al., Estimation of generalized mixtures and its application in image segmentation, IEEE Trans. Image Process. 6 (10) (1997) 1364–1375.
[33] C. Robert, G. Casella, Monte Carlo Statistical Methods, 2013.
[34] N. Metropolis, et al., Equation of state calculations by fast computing machines, J. Chem. Phys. 21 (6) (1953) 1087–1092.
[35] L. Younes, Parametric inference for imperfectly observed gibbsian fields, Probab. Theory Relat. Fields 82 (4) (1989) 625–645.
[36] B. Chalmond, An iterative Gibbsian technique for reconstruction of m-ary images, Pattern Recog. 22 (6) (1989) 747–761.
[37] E. Monfrini, W. Pieczynski, Estimation de mélanges généralisés dans les arbres de Markov cachés, application à la segmentation des images de cartons d'orgue de barbarie, Traitement du Signal 22 (2) (2005).
[38] J.G. Dias, M. Wedel, An empirical comparison of EM, SEM and MCMC performance for problematic Gaussian mixture likelihoods, Stat. Comput. 14 (4) (2004) 323–332.
[39] J. Gonzalez, et al., Parallel Gibbs sampling: from colored fields to thin junction trees, in: AISTATS, 2011, pp. 324–332.
[40] J. Besag, Statistical analysis of non-lattice data, Statistician (1975) 179–195.
[41] H. Derin, H. Elliott, Modeling and segmentation of noisy and textured images using Gibbs random fields, IEEE Trans. Pattern Anal. Mach. Intell. (1) (1987) 39–55.
[42] Pléiade website, 2017, (https://pleiades.cnes.fr/en).
[43] B. Rieger, L.J. Van Vliet, A systematic approach to nd orientation representation, Image Vis. Comput. 22 (6) (2004) 453–459.